PRELIMINARY VALIDATION OF ASAR GEOMETRIC ACCURACY

David Small, Adrian Schubert, Urs Krüttli, Erich Meier, Daniel Nüesch

Remote Sensing Laboratories, University of Zürich, Winterthurerstr. 190; CH-8057 Zürich, Switzerland,
Email:david.small@geo.unizh.ch

ABSTRACT/RESUME

We describe preliminary validation experiments performed to validate the geometric accuracy of ENVISAT ASAR data acquired in image (IM) and alternating polarisation (AP) modes. ESA's ASAR transponders in The Netherlands were used primarily as reference locations. Corner reflectors were deployed at test sites in Switzerland for comparison, and conventional ground control points such as bridges and road intersections were also used. The location of the reference points in radar geometry was predicted based upon the reflector's geographical position (and delay term in the case of transponders) and compared with the actual measured location in the image products. We form tentative conclusions on the residual error sources.

1. INTRODUCTION

Ensuring high geometric accuracy for ASAR products is vital to the ground segment, as overlays with independent information sources (typically in a map geometry) are only possible when the transformation between radar and map geometry is well calibrated. We describe validation steps undertaken to ensure that the transformations from radar to map geometry and back again are as accurate as possible. The ground segment of every new system must validate its geocoding chain to ensure that all parameters are treated consistently and are compatible with the product specifications [2]. Experiences with ERS-1 geopositional accuracy were reported in [5].

Special attention is devoted to the range and azimuth timing, as well as the cartographic and geodetic parameters describing the reference map projections and the orbit quality: FOS (flight operations segment) *predicted* (FP) and *restituted* (FR), DORIS *preliminary* (DOR_POR_AX) and *precise* (DOR_VOR_AX).

ASAR IMS and APS products are arranged in the radar's native slant-range geometry. IMP, APP, IMM, APM, and WSM products are provided in ground-range geometry, whereby the slant-range axis is replaced by a polynomial approximating equal ellipsoid range resolution across the swath. IMG and APG products are arranged in map geometry – they are ellipsoid-geocoded, i.e. terrain corrections are neglected. Each product type requires a special calibration and validation methodology.

The work presented here was performed within the ESA-DLR contract "*Contributions of RSL to the ERS-ENVISAT Ground Segment*".

2. METHODOLOGY

Each of the broad product types (slant-range, ground-range, and ellipsoid-geocoded) must be validated slightly differently. In the case of slant-range products, the positions of ground control points are predicted within the native radar geometry, while ground-range products require a further transformation in the range dimension. In the case of ellipsoid-geocoded products, a transformation is only required between the map projection of the image and that of the reference information.

2.1 Slant Range Products (IMS, APS)

The locations of the four ESA transponders within the Netherlands as well as their delays were used to predict the position, in range and azimuth coordinates, of their expected appearance within each product. The position of each transponder is first transformed from WGS84 geographic values into global Cartesian coordinates. The position along the orbit t_{az} is then found that satisfies the zero-Doppler condition, via Eqn. (1):

$$f_{D_{ref}} = 0 = \frac{2}{\lambda} \times \frac{(S-P)}{|S-P|} \times (v_p - v_s), \qquad (1)$$

where *P* is the transponder, *S* the spacecraft position in Cartesian space, and v_p and v_s are their respective velocities. The condition is solved using the orbital state vectors and timing parameters read from the product header annotations [2]. The "expected" range R_t of the transponder in the image is then calculated via Eqn. (2):

$$R_t = |S - P| + t_{Delay} \times \frac{c}{2}, \qquad (2)$$

where t_{Delay} is the transponder's delay, and *c* is the speed of light. The SLC image coordinates are then easily derived from t_{az} and R_t.

This "predicted" position was then compared with the actual measured location of the transponder within each image. Since the transponders are distributed across the Netherlands, not all appear within the bounds of every scene. For the visible transponders, the mean azimuth and range differences were calculated within each scene.

2.2 Ellipsoid-geocoded Products (IMG, APG)

Ground control points such as bridges, road, and canal intersections were measured within the ellipsoid-geocoded image and in reference topographic maps. Such comparisons are only meaningful for validation purposes in extremely flat areas, where large topography-induced displacements do not mask the much smaller residual biases within the geocoding system. IMG and APG products are typically delivered in a Universal Transverse Mercator (UTM) map projection, necessitating a transformation into the projection system of the topographic maps used for comparisons.

3. TEST SITES AND DATA AVAILABLE

Most of the data available were acquired over the Flevoland test site (52.5°N, 5.1°E). One product each was available covering the Bern (47.2°N, 7.5°E) and Bern-Zürich (47.3°N, 8.6°E) test sites in Switzerland.

The available IMG and APG data sets are summarized in **Table 1**. All products were processed on the ESRIN standalone processor (PF-ASAR v3.03S) unless otherwise indicated with the highest quality orbit state vectors available at the time. The table lists the product type, orbit number, beam, range-chirp type used during range compression, and differentiates between ascending and descending orbits. It also lists the annotations concerning the source of the orbit state vectors used during processing (orbit quality). Note that diversity in beam and ascending/descending configuration is assured.

Table 1 - ENVISAT ASAR—Available IMG & APG Flevoland Datasets

Product Type	*Orbit*	*Beam*	*Asc / Desc*	*Orbit Quality (MPH/DSD values)*	*Range Chirp Type*
IMG	3311	IS7	D	**FR**/DOR_POR_AX	Nominal
	3354	IS5	D	FP/DOR_POR_AX	
	3397	IS4	D	FP/DOR_POR_AX	
	3447	IS5	A	FP/DOR_POR_AX	
	3490	IS6	A	FP/DOR_POR_AX	
	3547	IS1	A	FP/DOR_POR_AX	
APG	3590	IS2	A	FP / -	Nominal
	3633	IS3	A	**FR**/DOR_POR_AX	
	3669	IS3	D	FP/DOR_POR_AX	
	3812	IS7	D	FP / -	
	3898	IS4	D	FP / -	

PF-ASAR v3.03S products are subject to an ambiguity in the annotations describing the state vectors used during processing. The main product header (*MPH*) contains an annotation labelled VECTOR_SOURCE, while a data set descriptor (*DSD*) within the specific product header (*SPH*) may or may not list a state vector filename used during processing. The column orbit quality in **Table 1** lists the two values as *<MPH Value> / <DSD Value>*. MPH values are typically either FP (flight segment *predicted* quality) or FR (flight segment *restituted* quality). DSD values are typically either blank, indicating that the MPH value should be interpreted at face value – we indicate this with a dash "–", DOR_POR_AX for DORIS *preliminary* quality, or DOR_VOR_AX for *precise* quality.

The IMS and APS products range compressed with nominal chirps available for the Flevoland test site are listed in **Table 2**. The improvements in comparison to chirp-replica based range compression were described in [6] and are not repeated here.

Table 2 - ENVISAT ASAR—Available IMS & APS Datasets

Test Site	*Product Type*	*Orbit*	*Beam*	*Asc / Desc*	*Orbit Quality* (MPH/DSD values)	*Range Chirp Type*
Flevoland	IMS	1894	IS4	D	FP/DOR_POR_AX	Nominal
		2209	IS2	D	FP/DOR_POR_AX	
		3311	IS7	D	FP/DOR_POR_AX	
Flevoland	APS	3583	IS6	D	FP / -	Nominal
		3590	IS2	A	FP / -	
		3712	IS2	D	FP / -	
		3812	IS7	D	FP / -	
		3855	IS5	D	FP / -	
		3898	IS4	D	FP / -	
Bern	APS	2810	IS2	D	FP / -	Nominal
Bern-Zürich		2853	IS2	D	FP / -	

4. ELLIPSOID GEOCODED PRODUCTS (IMG, APG)

Visualisations of sample image mode ellipsoid-geocoded (IMG) and alternating polarisation mode ellipsoid-geocoded (APG) products are shown in **Figure 1**. Ground control points were measured in the available IMG and APG Flevoland images, and compared with map measurements taken from 1:25000 and 1:50000 topographic maps. Such a validation test is only meaningful for ellipsoid geocoded products in extremely flat areas such as Flevoland. Given any significant terrain, topography-induced displacements mask any biases caused by systematic geocoding inaccuracies.

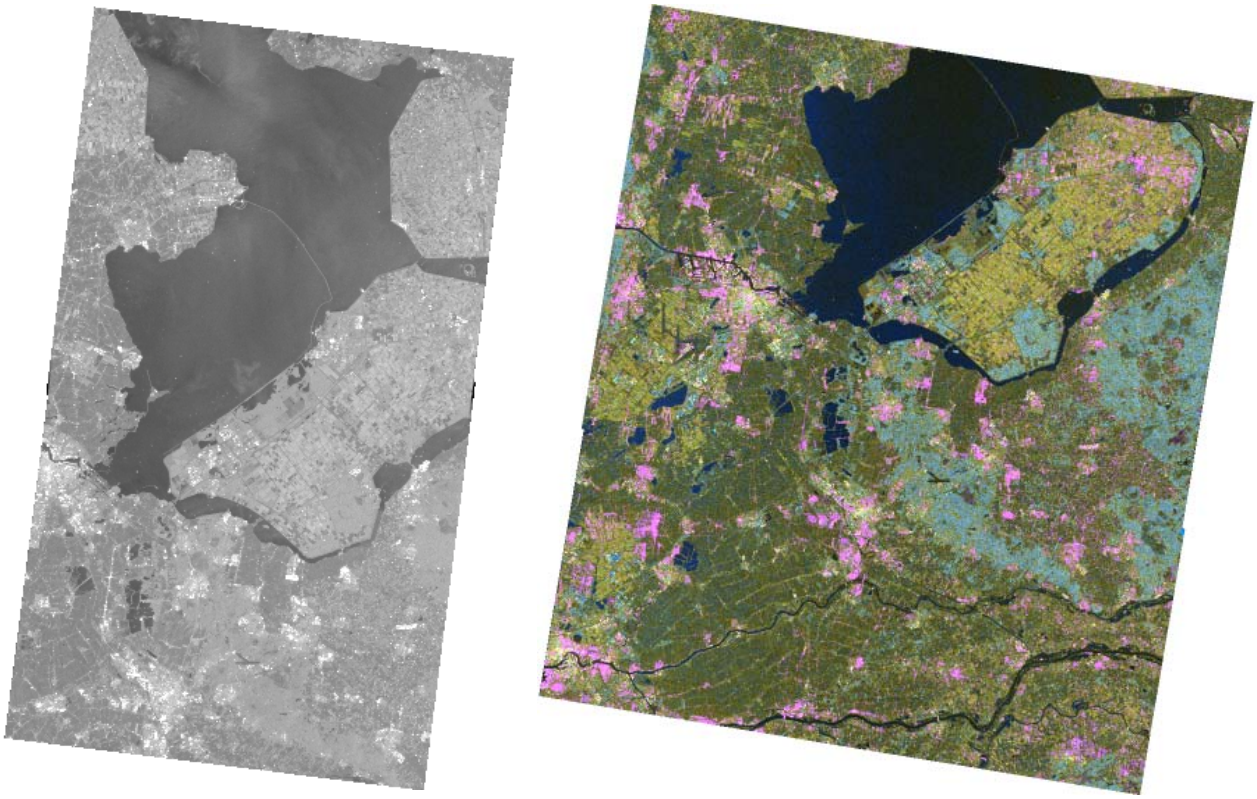

(a) IMG **(b) APG**

Figure 1: Flevoland IMG & APG Products: (a) IMG, orbit 3311, IS7 VV, (b) APG, orbit 3898, IS4 HH HV |HH-HV|

The image measurements were transformed from the product's UTM map projection into the Dutch stereographic map projection used by the topographic maps and compared to the map coordinates. The localisation accuracies measured are tabulated in **Table 3**. The mean and standard deviation of position differences are listed for the easting and northing axes. Note that although most accuracies are better than 50m, larger than normal deviations are found in the IMG orbit 3311 and APG orbit 3898 scenes. The deviations (more than 100m in each case) are mainly in the northing direction, and could be caused by inaccurate orbit state vectors having been used.

Table 3: Standard ESA ellipsoid geocoding IMG/APG localisation accuracy

Product	**Beam**	**Asc / Desc**	**Orbit Quality** *(MPH/DSD values)*	**Easting [m]**	**Northing [m]**
IMG-3311	IS7	D	**FR**/DOR_POR_AX	-7.4±5.8	-192.8±10.8
IMG-3354	IS5	D	FP/DOR_POR_AX	6.9±5.8	-13.4±5.5
IMG-3397	IS4	D	FP/DOR_POR_AX	20.0±30.3	-19.8±13.1
IMG-3447	IS5	A	FP/DOR_POR_AX	1.2±19.9	26.3±13.8
IMG-3490	IS6	A	FP/DOR_POR_AX	-3.0±16.2	16.0±11.9
IMG-3547	IS1	A	FP/DOR_POR_AX	-35.3±26.7	9.7±9.2
APG-3590	IS2	A	FP / -	-20.5±23.6	-47.0±14.3
APG-3633	IS3	A	**FR**/DOR_POR_AX	-5.7±10.6	19.0±11.0
APG-3669	IS3	D	FP/DOR_POR_AX	28.5±22.6	-18.4±19.1
APG-3812	IS7	D	FP / -	11.6±8.7	-4.8±11.9
APG-3898	IS4	D	FP / -	36.6±15.5	124.4±13.8

5. PREDICTION OF RADAR GEOMETRY IMAGE LOCATION

5.1 Switzerland

The Remote Sensing Laboratories (RSL) of the University of Zürich conducted a ground truth campaign between May and Nov. 2002, orienting corner reflectors within multiple test sites in Switzerland for ENVISAT overpasses. **Figure 2** shows three of the corner reflectors deployed in the field during the campaign.

Emmen Dübendorf Payerne

Figure 2 – Swiss ASAR Corner Reflector Campaign 2002

Two alternating polarisation single look complex (APS) products were available from the time of the corner reflector campaign. Visualisations of the products are shown in **Figure 3**(a). A sampling window start time (SWST)-change artefact is visible in the area adjacent to SWST-change. The problem was solved by ESA with a software upload to the ASAR instrument on Nov. 11, 2002. All ASAR data acquired after that date should not be subject to the problem. The locations of the corner reflectors in the slant range images are marked.

Figure 3(b) shows close-ups of the corner reflectors within each scene. Multiple zoom levels are shown, always centred on the predicted location in radar geometry calculated from the differential-GPS surveyed corner reflector position and the orbit state vector annotations. In the top row, a synoptic overview of the neighbourhood with three range looks and 15 azimuth looks is shown. Below that, a more local image at one range look by five azimuth looks is shown. Finally, in the bottom row, the neighbourhood surrounding the predicted location is shown at the native single look complex (SLC) resolution of the detected image. The corner reflectors are weakly visible in both full resolution images, with similar biases to the predicted location (shifted to the lower left). Note that all radar geometry images in

Figure 3 have been mirrored in the range dimension to ease identification of ground features. **Figure 3**(c) shows the terrain-geocoded product using nominal imaging geometry parameters. The same SWST-change artefact is visible. For an end-to-end system test, ground control points were also measured within the terrain-geocoded images, and compared to map locations in the Swiss oblique Mercator map projection. The mean and standard deviation of the differences are listed in **Table 4**. This represents an excellent accuracy in the absence of any refinement of imaging parameters, although the *predicted*-quality orbit state vectors used would not guarantee such results in every case. **Table 5** shows the differences between the predicted and measured image locations for the three corner reflectors present in the two scenes. The sign and magnitude of the range bias is consistent with later results from the Netherlands.

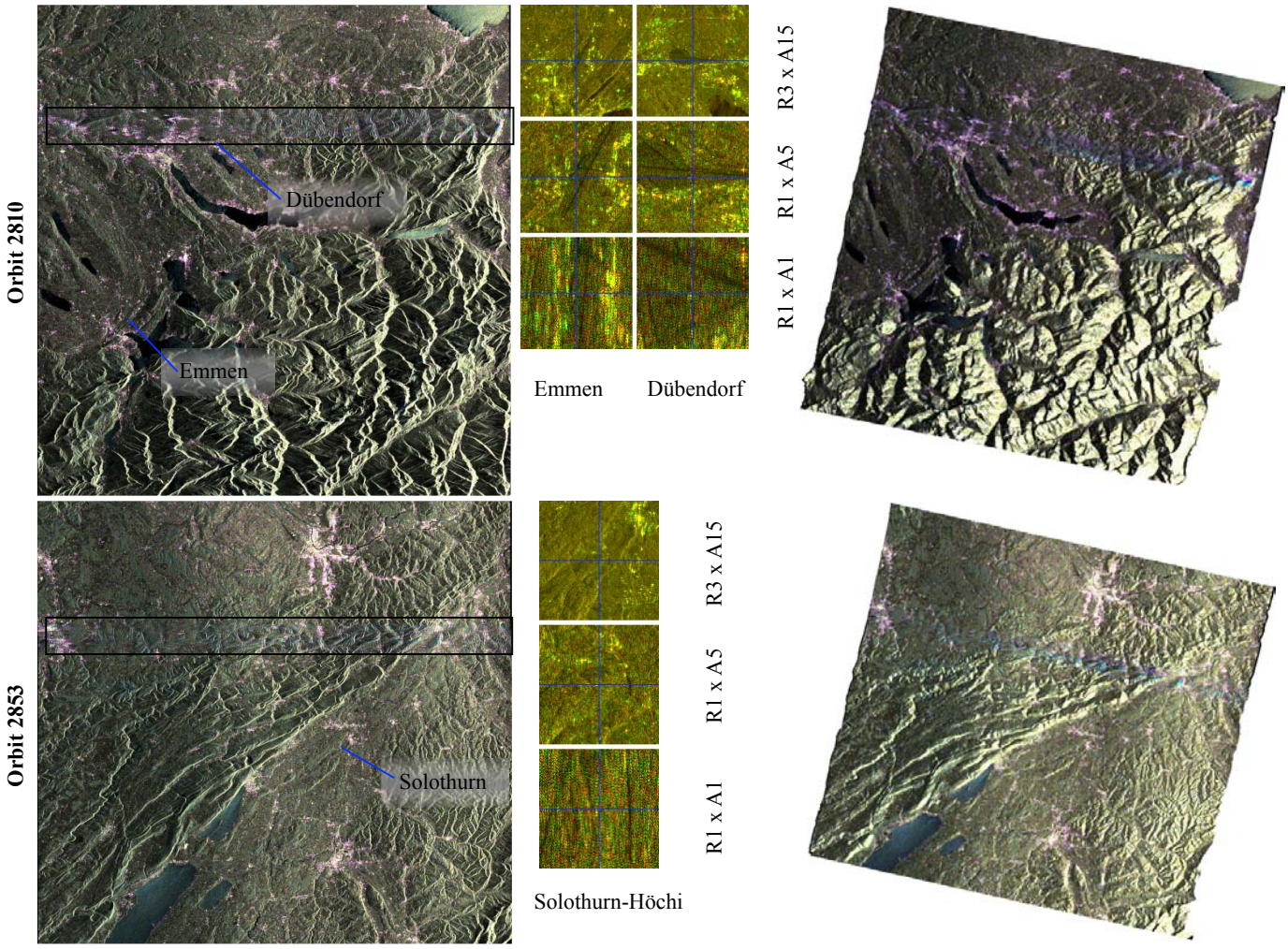

Figure 3 – APS products from Swiss test sites (range-mirrored): (a) slant-range VV, HH, |VV-HH|; (b) Corner reflector location predictions VV, HH, Prediction; (c) terrain-geocoded APS products VV, HH, |VV-HH|

Table 4 – Terrain-geocoding geolocation accuracy for Swiss test sites

Product	**Beam**	**Orbit Quality** *(MPH/DSD values)*	**Easting [m]**	**Northing [m]**
APS-2810	IS2 D	FP / -	-27.3±25.7	-18.0±14.6
APS-2853	IS2 D	FP / -	-40.5±20.4	-17.2±16.6

Table 5 – Predicted vs. measured image locations for Swiss corner reflectors

Product	Beam	Orbit Quality *(MPH/DSD values)*	Corner Reflector	Azimuth Difference [SLC samples]	Range Difference [SLC samples]
APS-2810	IS2 D	FP / -	Dübendorf	-2.4	-2.5
			Emmen	-2.6	-2.9
APS-2853	IS2 D	FP / -	Solothurn	-3.7	-3.0

5.2 The Netherlands

Transponder locations were provided in WGS84 geographic coordinates together with their individual delay estimates. These coordinates were combined with the provided orbit state vectors to predict range and azimuth locations within each image product. Most products contained less than the full complement of four ESA transponders, as some transponders were outside the product's geographic footprint. In a few other cases, a transponder was nominally within the acquisition area, but did not respond. The Edam and Swifterbant transponders are located closer to the centre of the Flevoland test site area, and were acquired more often than the Zwolle and Aalsmeer transponders.

5.2.1 IMS

The IMS products studied are shown in **Figure 4**. For the three products, the predicted transponder locations are marked with a blue cross on the actual image products, illustrated with multi-look factors of three, one, and one range-looks, and fifteen, five, and one azimuth looks – see **Figure 4**(a). The actual transponder location is apparent in each sub-image from the strong response, including considerably extended range and azimuth sidelobes (aside from Zwolle in IMS-2209, that appears not to have responded). The transponder location was measured in a highly (≥20x) oversampled version of the image region to attain sub-pixel accuracy.

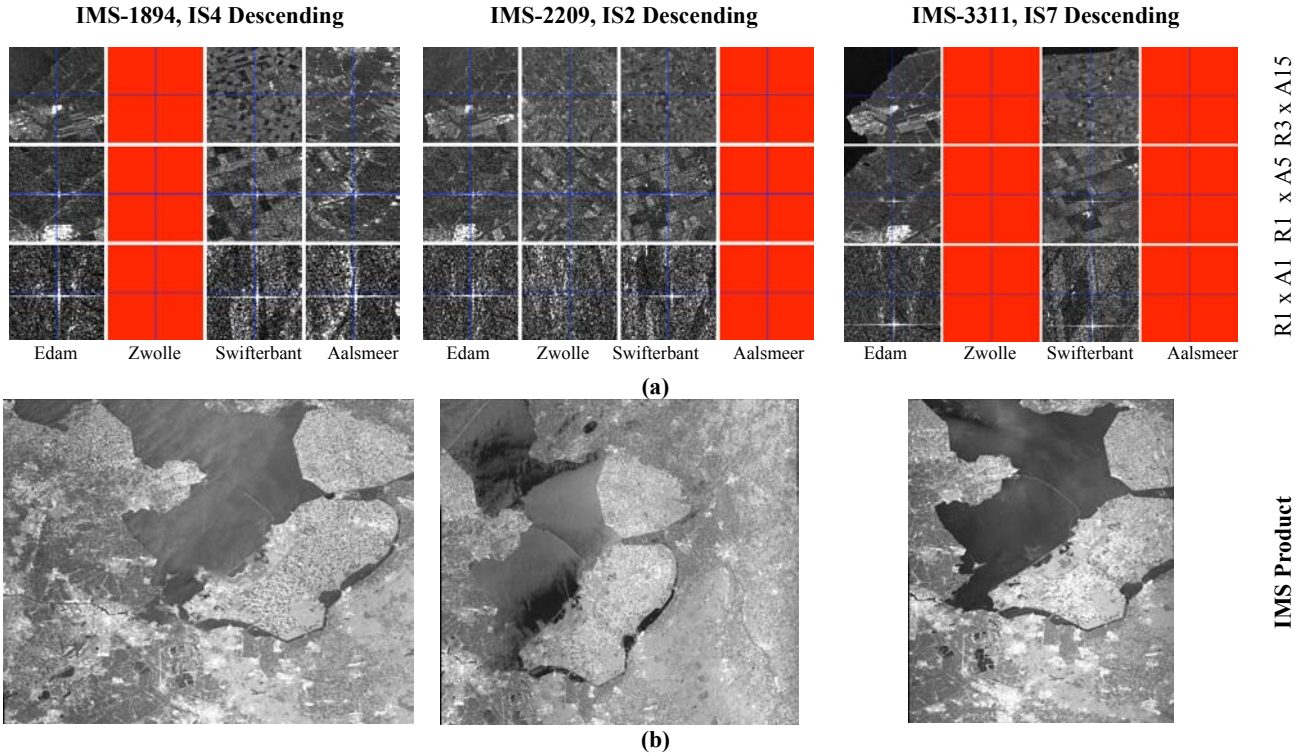

Figure 4 – Flevoland IMS Products & Transponder Location Predictions: (a) Juxtaposition of predicted and actual/measured transponder locations (red indicates out of image); (b) Associated IMS slant-range images

Note that the predictions and measurements agree extremely well in the cases of orbits 1894 and 2209, but much less so for orbit 3311, particularly in the azimuth direction. In the case of IMS-3311, the size of the neighbourhood window even had to be increased to show the actual location. Overviews of the three IMS products are shown in **Figure 4**(b). The large azimuth differences between predicted and measured image locations for the IMS–3311 product were probably caused by a poor accuracy of the *preliminary*-quality orbit state vectors available (possibly due to orbit

manoeuvres around that time), although this requires further investigation. The MPH & DSD headers were the same for all three products, as listed in **Table 2**. Quantitative differences between predicted and measured range and azimuth coordinates are listed in **Table 6** for each transponder, improved since [6]. Note the high degree of consistency for single-transponder results, suggesting possible residual inaccuracies in the transponder position and/or delay information. The large azimuth error detected in product IMS-3311 is consistent with the large northing deviation measured in the IMG-3311 product documented in **Table 3**.

Table 6 – Flevoland IMS Transponder Locations – Prediction vs. Measurement

Product	**Beam**	**Orbit Quality** *(MPH/DSD values)*	**Transponder**	**Azimuth Difference [SLC samples]**	**Range Difference [SLC samples]**
IMS-1894	IS4	FP/DOR_POR_AX	Edam	-4.39	-3.70
			Swifterbant	-5.79	-4.02
			Aalsmeer	-4.29	-2.83
IMS-2209	IS2	FP/DOR_POR_AX	Edam	-3.85	-3.68
			Swifterbant	-5.13	-4.01
IMS-3311	IS7	FP/DOR_POR_AX	Edam	-62.31	~~-3.16~~
			Swifterbant	-64.47	~~-3.48~~

5.2.2 APS

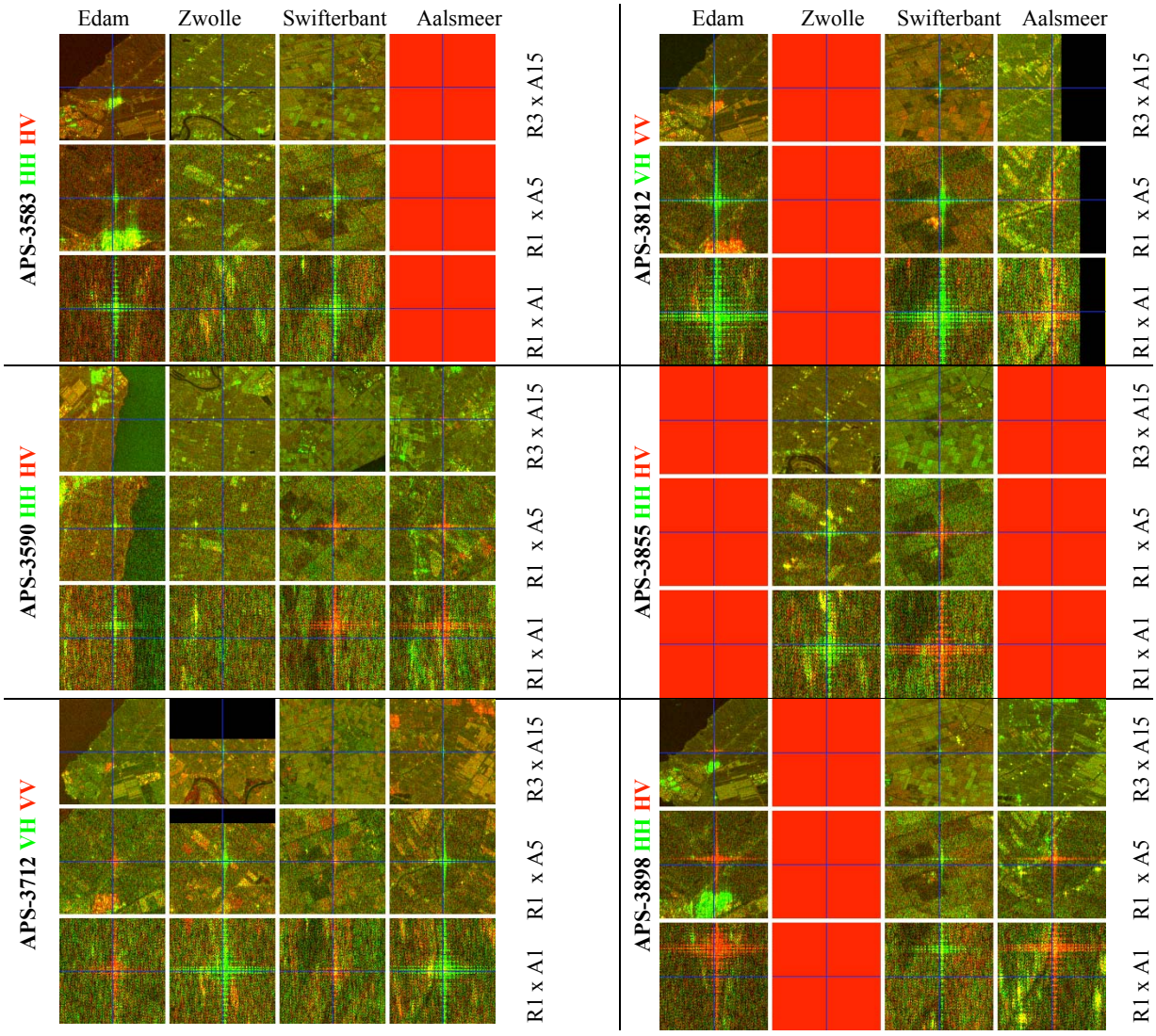

Figure 5 – Transponder neighbourhoods in Flevoland APS products juxtaposing predicted and measured locations – red indicates that transponder was out of image – ESA ASAR transponders return a single polarisation

The neighbourhoods surrounding the predicted range and azimuth radar image coordinates of the APS products are shown in **Figure 5**, again with multi-look factors of three, one, and one in range, and fifteen, five, and one in azimuth. The images are shown in colour (one polarisation each for red and green) to highlight the returns in both of the AP–mode polarisations. The ASAR transponder Zwolle appears not to have responded in the products from orbits 3583 and 3590. The disjoint structure of each transponder's sidelobes is an artefact of the ScanSAR nature of the acquisition mode. Cross talk between polarisations appears to be reasonably low, as contamination of the non-activated polarisation is not strong.

Quantitative differences between predictions and measurements for the six APS products, averaged over all present transponders, are listed in **Table 7**. Five descending and one ascending APS scene were available: all products were annotated with *predicted* orbit quality. In addition to the transponder measurements, for all six APS products, ground control points were measured both in 4-look detected slant-range images and in 1:25000 or 1:50000 Dutch topographic map sheets. In the case of map GCPs, both mean and standard deviation of the bias estimates are provided. The low number of transponder measurements available do not allow for standard deviation estimates. Considerable agreement exists between the transponder and GCP-based results, with the single ascending scene marking the only significant departure from the norm. Differences may possibly be due to a bias in projection parameters and datum shift values, as well as scene-height variations not present in surveyed transponder WGS84 coordinates. More scenes with ascending geometries need to be studied to form definitive conclusions. No strong beam-dependent range bias was detected.

Table 7 – Flevoland APS Localisation Accuracies

Product	**Beam & Orbit Configuration**	**Orbit Quality** *(MPH/DSD values)*	**Azimuth Predicted – Measured Difference [SLC samples]**		**Range Predicted – Measured Difference [SLC samples]**	
			Transponders	Map GCPs	Transponders	Map GCPs
APS-3583	IS6 D	FP / -	-0.01	-0.8±1.8	-3.95	-3.0±0.8
APS-3590	IS2 A	FP / -	15.03	9.7±3.2	-3.43	-3.5±0.8
APS-3712	IS2 D	FP / -	0.57	-0.6±4.7	-2.83	-1.9±1.4
APS-3812	IS7 D	FP / -	-5.52	-5.8±3.5	-3.20	-2.3±0.7
APS-3855	IS5 D	FP / -	-5.93	-5.6±3.1	-3.30	-2.9±0.9
APS-3898	IS4 D	FP / -	33.55	33.0±2.6	-3.36	-2.9±0.7

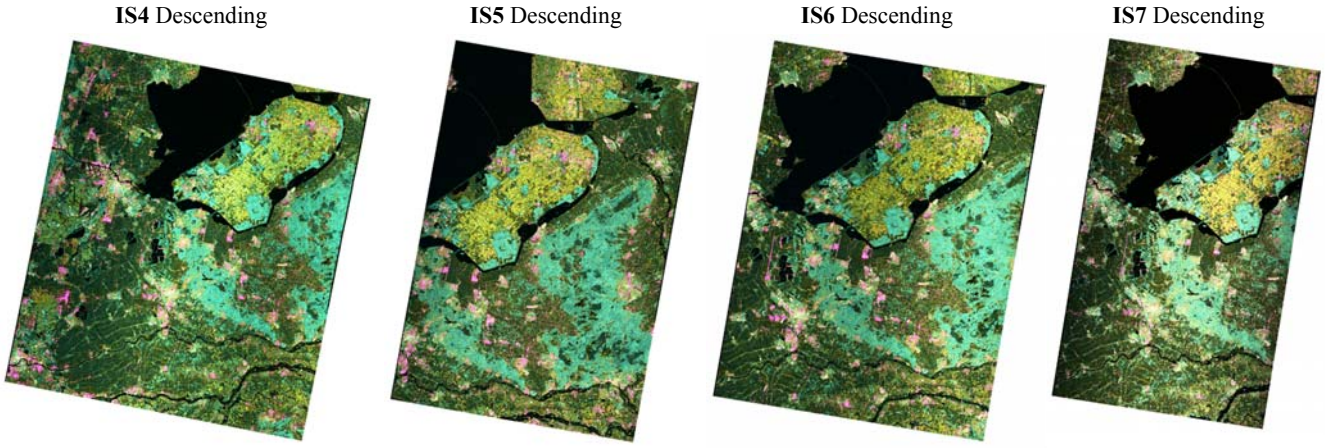

Figure 6 –GLOBE DEM non-refined "Terrain"-geocoded Flevoland APS images (IS4-IS7)

As an end-to-end system test, the APS scenes were geocoded using the nominal header values for near range and first azimuth time etc., and a GLOBE 1km resolution DEM oversampled to 12.5m sampling. Overviews of four of the geocoded APS products (IS4-IS7) are shown in **Figure 6**. One sees that the simultaneous availability of co-pol and cross-pol returns enables discrimination between different land-cover types.

One qualitative test of the accuracy of a geocoding system is an overlay of two independently geocoded products. We performed such a test by overlaying the co-pol VV return of the geocoded APS-3812 with the cross-pol HV return from the geocoded APS-3855 product. The result is shown in **Figure 7**. No significant shifts between the two results are

readily apparent, even when viewed at a 12.5m sampling interval. The geometric accuracy is sufficiently high to make the overlay difficult to distinguish from a single-product AP dual-polarisation visualisation, such as those shown in **Figure 6**.

Flevoland Area

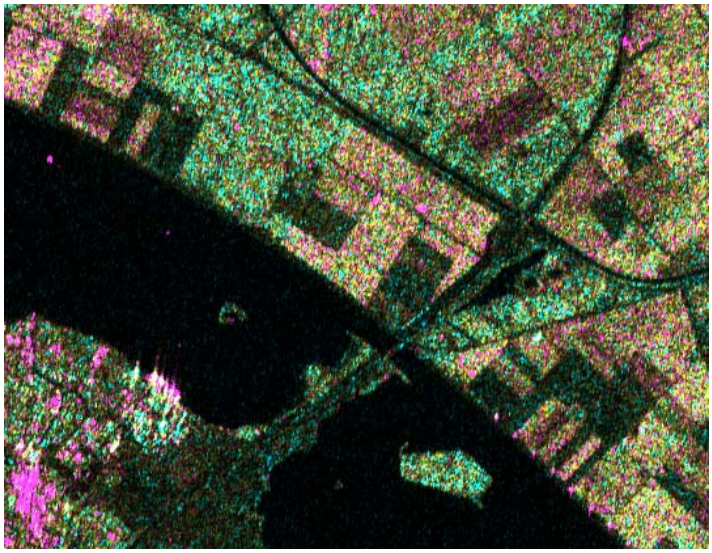

12.5m Sampling

Figure 7 – GLOBE DEM non-refined "Terrain"-geocoded overlay performed using nominal header geometry parameters of APS–3812 VV (IS7 Descending) and APS–3855 HV (IS5 Descending), |HV-VV|

A more quantitative end-to-end test of localisation accuracy is provided in **Table 8**, where the means and standard deviations of ground control points measured within the APS-GTC images are listed. Note that the geocoding was performed without any refinement – only the nominal header-provided information was used throughout. The localisation accuracy is generally quite acceptable, with only the products from orbits 3590 and 3898 having significant biases. Their departures from the norm were also observed via the azimuth and range differences calculated from transponder and slant-range GCP measurements listed in **Table 7**.

One can compare these results with the earlier APG localisation tests for the intersection of the product sets (orbits 3590, 3812, and 3898). Comparing **Table 3** and **Table 8**, one sees that the APS geocoding is slightly less accurate, particularly in the ascending case. Since the APS products are geocoded to the Dutch map projection, they may be subject to a datum shift bias not present in the standard UTM projection WGS84-based APG products. The disparity could be caused by differing orbit state vectors in the respective product headers. Both the APG and APS products were annotated with orbits of identical poorest quality *predicted* type (main product header FP annotation), but the state vectors themselves differ slightly between APS and APG for the same orbit. Future investigations of product series processed with identical (ideally *precise*-quality) state vectors will allow clearer comparisons.

Table 8 – APS end-to-end localisation accuracy

Product	**Beam**	**Orbit Quality** *(MPH/DSD values)*	**Easting [m]**	**Northing [m]**
APS-3583	IS6 D	FP / -	-32.4±8.0	4.0±7.0
APS-3590	IS2 **A**	FP / -	**76.7**±12.2	-20.7±10.4
APS-3712	IS2 D	FP / -	-34.5±18.0	3.8±14.0
APS-3812	IS7 D	FP / -	-25.1±9.4	-12.6±8.2
APS-3855	IS5 D	FP / -	-32.3±15.0	-2.9±14.8
APS-3898	IS4 D	FP / -	-6.7±18.9	**135.3**±10.8

6. SUMMARY, CONCLUSIONS, AND OUTLOOK

The problem of significant range-biases in all product types were corrected by using nominal chirp references rather than chirp replicas during range compression.

Localisation accuracy of (non-refined / a-priori) terrain-geocoded IM and AP products was generally excellent, even with sub-optimal state vector quality available. However, some scenes suffered from larger errors, usually in azimuth, even with relatively good *preliminary*-quality annotation, possibly caused by adjacent orbit manoeuvres, but further investigation is required.

There is broad agreement between results from transponder and map-based GCP measurements, and end-to-end terrain-geocoding system validation tests. The cause of relative biases between transponder measurements may be due to uncertainty in the transponder locations and/or delay values, but requires further investigation. A range bias of consistent sign was determined. Across multiple test sites, the value is nearly constant for both ascending and descending geometries, indicating that the bias is likely systematic to the radar geometry. No strong beam-dependent sampling window start time bias was found. No significant difference in geometric accuracy was observed between IM and AP modes.

Slightly different APS and APG geocoding accuracies are likely due to differing input state vectors used. Future investigations will ideally use consistent state vector sources. Improved quality state vectors (i.e. DORIS-*precise* orbits, or even more regular inclusion of DORIS-*preliminary* quality products) in ASAR products will be necessary for definitive conclusions on ASAR's geometric performance, and calibration/validation of the sampling window start time bias.

7. ACKNOWLEDGMENTS

The authors wish to gratefully acknowledge the assistance from Manfred Zink, Josep Closa, and Betlem Rosich of ESA, and Jürgen Holzner, Birgit Schättler and Detlev Kosmann of DLR, and Hannes Raggam of Joanneum Research for useful discussions.

8. REFERENCES

[1] ASAR Cal/Val Team, *ASAR Cal/Val Implementation Plan*, Issue 1.0, March 2002.

[2] ENVISAT Payload Data Segment, *ENVISAT Products Specification - Volume 8: ASAR Products Specifications*, Jan. 2002.

[3] J. Closa, *Processor Verification*, ENVISAT Calibration Review, ESTEC, Noordwijk, The Netherlands, Sept. 2002.

[4] D. Kosmann, J. Holzner, W. Hummelbrunner, D. Small, *Geometric Accuracy of ASAR Products – Calibration Phase*, Proc. EUSAR 2002, Cologne, Germany, June 4-6, 2002, pp. 471-474.

[5] A. Roth, T. Hügel, D. Kosmann, M. Matschke, G. Schreier, *Experiences with ERS-1 SAR geo-positional accuracy*, Proc. IGARSS'93, Tokyo, Japan, pp. 1450-1452.

[6] D. Small, D. Kosmann, J. Holzner, J. Raggam, M. Pirri, A. Schubert, U. Krüttli, W. Hummelbrunner, M. Franke, *ASAR Level 1 Geolocation*, Proc. of ENVISAT Calibration Review, ESA-ESTEC, Noordwijk, The Netherlands, Sept. 9-13, 2002.

[7] D. Small, S. Biegger, D. Nüesch, *Automated tiepoint retrieval through heteromorphic image simulation for spaceborne SAR sensors*, Proc. of ERS-ENVISAT Symposium, ESA Publication SP-461, Gothenburg, Sweden, Oct. 16-20, 2000.

[8] M. Zink, *ASAR Calibration Review Introduction*, ENVISAT Calibration Review, ESTEC, Noordwijk, The Netherlands, Sept. 2002.